

PULSAR SCINTILLATION ARCS. I. FREQUENCY DEPENDENCE

ALEX S. HILL, DANIEL R. STINEBRING, HENRY A. BARNOR,
 DANIEL E. BERWICK, AND AARON B. WEBBER

Department of Physics and Astronomy, Oberlin College, Oberlin, OH 44074

Received 2003 June 11; accepted 2003 August 20

ABSTRACT

Dynamic spectra of pulsars often show low-level crisscross patterns as well as isolated interference maxima called scintles. Previously, we have shown that a power spectrum analysis of the dynamic spectrum usually exhibits a parabolic arc with a well-determined curvature. A simple analysis predicts that this curvature should scale with observing frequency as ν^{-2} . We report on multifrequency observations of three pulsars at the Arecibo Observatory that are designed to test this prediction and explore the frequency behavior of the power distribution. We find that the arc curvature scales as expected over more than a factor of 5 in observing frequency (0.43–2.2 GHz). This allows us to compare arc curvature at different frequencies obtained over a long time span. Furthermore, we find that scintillation arcs are a broadband phenomenon: they are present contemporaneously, and with the same general appearance, over a wide frequency range. At higher frequencies ($\gtrsim 1$ GHz) the arcs are more sharply defined, substructure is more prominent, and inverted subarcs often appear with vertices along the main parabola.

Subject headings: ISM: general — ISM: structure — pulsars: general

1. INTRODUCTION

There is only partial understanding of the production, maintenance, and dissipation of turbulence in the interstellar medium (ISM; e.g., Norman & Ferrara 1996). Since radio waves are scattered by electron inhomogeneities in the ISM (Scheuer 1968; Rickett 1990), pulsar scintillation observations of various kinds provide a valuable probe of turbulence in the Galactic disk. By combining observations of diffractive scintillation, refractive scintillation, and fluctuations in dispersion measure and rotation measure, Armstrong, Rickett, & Spangler (1995) provided evidence for a Kolmogorov spectrum over the range 2×10^6 m to 10^{13} m, and this spectrum may extend over a remarkable ~ 12 orders of magnitude in size. There is no consensus, however, on how this large inertial subrange is maintained and dissipated, what phase of the ISM is primarily responsible for the scintillation effects observed, how the material is distributed along the line of sight, or the relation between stochastic turbulence and deterministic structures.

Even after 30 years of study, new aspects of pulsar scintillation are being uncovered. Loosely organized crisscross features in pulsar dynamic spectra were noticed in early observations (Hewish, Wolszczan, & Graham 1985 and references therein), but they have only recently been shown to produce faint but high Q features in the secondary spectrum¹ (Stinebring et al. 2001, hereafter S01). Since the discovery of these “scintillation arcs” (parabolic features in the secondary spectrum), we have explored their variations in time and frequency for a variety of pulsars. In this paper we concentrate on the behavior of scintillation arcs with observing frequency.

This is the first in a series of papers exploring the scintillation arc phenomenon. D. R. Stinebring et al. (2003, in preparation; hereafter S03) present an observational overview of the phenomenon using a large set of obser-

uations from 1984 to 2003. B. J. Rickett et al. (2003, in preparation; hereafter R03) develop the theory of scintillation arcs. The primary intent of this paper is to explore scintillation arcs at multiple frequencies quasi-simultaneously, seeking answers to several questions: Are scintillation arcs a broadband phenomenon? Does the arc curvature scale with frequency as predicted by a simple thin-screen model? How does substructure in the arc change as the observing frequency is varied?

We investigate these questions with data from a 2 week observing run at the Arecibo Observatory² in 2002 June. In § 2 we review the basic model introduced in S01 and discuss the expected frequency dependence of scintillation arcs. In § 3, we present our observations. In § 4 we analyze the curvature of the scintillation arcs at multiple frequencies; and we discuss our conclusions in § 5.

2. A MODEL FOR ARC PRODUCTION

The dynamic spectrum is a measure of flux density as a function of frequency and time: $S(\nu, t)$. It contains information about differential delays and differential Doppler shifts between rays that make up the image of the pulsar on the sky (R03). The secondary spectrum is $P(f_\nu, f_t) = |S^\dagger(\nu, t)|^2$, where the \dagger denotes a two-dimensional Fourier transform. The axes of the secondary spectrum are conjugate time, f_t , and conjugate frequency, f_ν ; they are given by (S01; R03)

$$f_t = \left(\frac{D}{\lambda D_s} \right) (\theta_2 - \theta_1) \cdot \mathbf{V}_{\text{eff}, \perp}, \quad (1)$$

$$f_\nu = \left[\frac{D(D - D_s)}{2cD_s} \right] (\theta_2^2 - \theta_1^2), \quad (2)$$

²The Arecibo Observatory (<http://www.naic.edu>) is a part of the National Astronomy and Ionosphere Center, which is operated by Cornell University under a cooperative agreement with the National Science Foundation.

¹The secondary spectrum is the power spectrum of the dynamic spectrum.

where θ_1 and θ_2 are two points on the image in a coordinate system centered on the pulsar. The distance to the pulsar is D , and D_s is the distance from the pulsar to the scattering screen; c is the speed of light, and λ is the observing wavelength. The appropriately weighted velocity (only transverse components are relevant) is given by (Cordes & Rickett 1998)

$$\mathbf{V}_{\text{eff},\perp} = (1 - \sigma) \mathbf{V}_{p,\perp} + \sigma \mathbf{V}_{\text{obs},\perp} - \mathbf{V}_{\text{screen},\perp}, \quad (3)$$

where $\sigma \equiv D_s/D$ is the fractional distance from the pulsar ($\sigma = 0$) to the observer ($\sigma = 1$).

Motivated by the widespread appearance of parabolic features in high-sensitivity secondary spectra, we explore the case in which the image consists of a compact core at the origin of the image (location of the pulsar) and a substantially weaker extended halo.³ We fix one point at the origin, $\theta_1 = 0$, and orient the θ_x -axis of the image plane along the direction of the effective velocity of the pulsar. Omitting constants for clarity, we then have that

$$f_\nu \propto \theta_2^2 = \theta_{2x}^2 + \theta_{2y}^2, \quad (4)$$

$$f_i \propto \theta_{2x}, \quad (5)$$

so

$$f_\nu = a f_i^2 + b \theta_{2y}^2. \quad (6)$$

Rewriting equation (6) with the constants, considering interference between a point along the θ_x -axis ($\theta_{2y} = 0$) and a point at the origin, and making the assumption that the velocity of the pulsar is much greater than the velocity of the observer or the screen,⁴ $\mathbf{V}_{\text{eff},\perp} = (1 - \sigma) \mathbf{V}_{p,\perp}$, and

$$f_\nu = \frac{D\lambda^2}{2cV_{p,\perp}^2} \left(\frac{\sigma}{1 - \sigma} \right) f_i^2. \quad (7)$$

This shows that interference between a point along the θ_x -axis and a point source at the origin will give rise to a parabola in the secondary spectrum of the form $f_\nu = a f_i^2$, where the curvature parameter a is given by

$$a = \frac{D\lambda^2}{2cV_{p,\perp}^2} \left(\frac{\sigma}{1 - \sigma} \right). \quad (8)$$

Interference between any point not on the θ_x -axis ($\theta_{2y} \neq 0$) and the origin will add a $\theta_{2y}^2 > 0$ term to equation (7), leading to power *within* the parabola, so the parabola bounds power in the secondary spectrum in the case of a small, bright core at the geometrical location of the pulsar interfering with an extended halo.

The localization of scattering in a thin screen is an essential element of this model for the production of scintillation arcs. Only when the scattering occurs in a small region along the line of sight is there a linear dependence of f_i on θ , and a dependence of f_ν on θ^2 . As the thickness of the scattering

screen is increased, this relationship will change from a strictly deterministic one to a statistical one; the correlation between the two quantities may even approach zero for ray trajectories that are highly scattered (i.e., are essentially random walks with many changes of direction along the path).

This simple model can be expanded to include interference between two image points, multiple bright spots in the image, an asymmetrical halo, or numerous other modifications; we do so in other papers in this series. However, all of these image geometries leave the central parabolic arc in the secondary spectrum intact in some form. Moreover, a large number of observations show characteristics remarkably similar to those predicted by the simple core-halo interference model developed here. Here we concentrate on observations with relatively simple scintillation arcs because we can compare the properties of the arc at different observing frequencies more directly and easily.

3. OBSERVATIONS

We observed with the Arecibo telescope using essentially the same techniques employed in S01. Observations were made at center frequencies ranging from 430 to 2200 MHz, with observing bandwidths from 10 to 100 MHz (generally 10–12.5 MHz at 430 MHz, and 50 or 100 MHz at higher frequencies). We used the Gregorian 430 MHz, the L-wide (1.15–1.73 GHz), and the S-low (1.8–3.1 GHz) receivers. Most spectra were recorded with the Wideband Arecibo Pulsar Processor⁵ autocorrelation-based spectrometer. Some observations with a 10 MHz bandwidth used the Arecibo Observatory Fourier Transform Machine⁶ spectrometer. Two circular polarizations (for the 430 MHz receiver) or two linear polarizations (for the L-wide and S-low receivers) were summed in hardware to produce spectra with 1024 frequency channels every ≈ 4.1 ms. We then distributed spectra into 128 phase bins over the pulsar period using TEMPO (Taylor & Weisberg 1989) with an integration time of 10 s. This results in a cube of power as a function of time (10 s blocks), frequency, and pulsar phase. For each 10 s interval, we subtracted the off-pulse spectrum from the on-pulse spectrum to remove the background power and the most serious radio frequency interference; we then divided by the off-pulse spectrum to flatten the baseline. The result is a single column in the two-dimensional dynamic spectrum, and this is continued for the duration of the observation (typically 30–60 minutes). We then calculated the Fourier transform of the dynamic spectrum after applying a taper function to the highest and lowest 100 frequency channels of the 1024 channel dynamic spectra (leaving most of the band unaffected) in order to limit sidelobe structure along the conjugate frequency axis. The secondary spectrum is the squared modulus of the transformed dynamic spectrum.

The Nyquist frequency along the conjugate time axis was 3.0 cycles minute⁻¹ and ranged from 5.1 to 51.2 cycles MHz⁻¹ along the conjugate frequency axis. In most of our secondary spectra, the power falls off below the background noise well below the Nyquist frequency, indicating that our channel bandwidth is small enough that we are sensitive to the finest periodicities contained in the dynamic spectra.

³ We refer schematically to the core and the halo of the image. In fact, however, the image is continuous, and there is not a clear dividing line between components in most images. Such an image naturally arises from scattering in a turbulent medium with a Kolmogorov turbulence spectrum (R03).

⁴ This is the usual case for pulsars, which typically have transverse velocities much greater than the 30 km s⁻¹ orbital speed of the Earth. One pulsar in our sample, PSR B1929+10, has a relatively low transverse velocity, which we comment on further below.

⁵ See <http://www.naic.edu/~wapp>.

⁶ See <http://www.naic.edu/~aofm>.

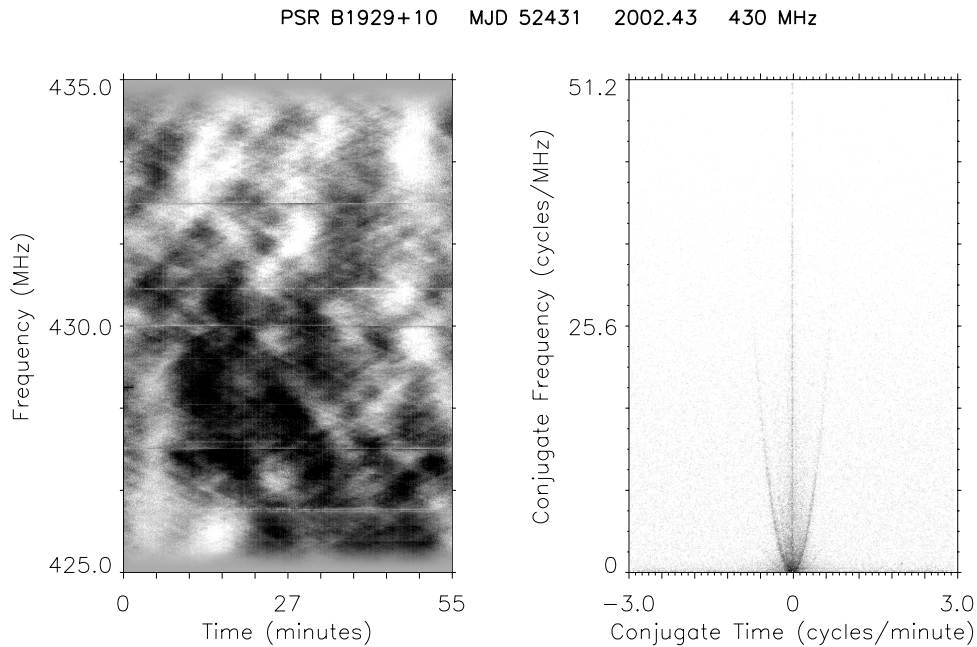


FIG. 1.—Typical dynamic (*left*) and secondary (*right*) spectrum pair, this one of PSR B1929+10 at 430 MHz. Periodic fringing in the dynamic spectrum gives rise to the sharply defined parabolic arc in the secondary spectrum, with power inside the parabola but very little power outside. The gray scale for the dynamic spectrum is linear in flux density. As in the other figures, the gray scale for the secondary spectrum is *logarithmic* in spectral power and extends from 3 dB above the noise floor to 5 dB below the maximum power level (see Rickett et al. 1997 for more details). A taper function applied to the dynamic spectrum limits sidelobe structure in the secondary spectrum; the window can be seen at the highest and lowest frequencies in the dynamic spectrum.

However, we must be alert to the possibility of missing high-frequency periodic fringing that is not contiguous with lower frequency features (Rickett, Lyne, & Gupta 1997).

The primary data source for this paper is a 2 week observing run in 2002 June, although we supplement these data with some observations from 2001 and the rest of 2002 when necessary. We observed eight pulsars (PSRs B0823+26, B0834+06, B0919+06, B1133+16, B1737+13, B1919+21, B1929+10, and B2016+28) during 18 sessions in 2002 June. Most pulsars were observed multiple times at three or more frequencies over the 2 week observing run; we often made observations of a given pulsar at two frequencies on consecutive days or in consecutive hour-long observations. A typical dynamic-secondary pair is shown in Figure 1; many similar observations are shown in S03. Parabolic arcs were clearly visible at multiple frequencies in our observations for all pulsars observed in 2002 June. The arcs were particularly well defined for pulsars B0834+06, B1133+16, and B1929+10. Secondary spectra for each of these pulsars at multiple frequencies are shown in Figures 2–4. In the remainder of this paper we focus on these three pulsars and analyze their behavior as a function of frequency.

4. ANALYSIS

4.1. *Qualitative Changes with Frequency*

We are interested in the instantaneous bandwidth of the scintillation arc phenomenon. It would be desirable to have simultaneous observations over a wide bandwidth, but that is technically challenging. However, we have seen in these and previous observations (S03) that the main features of an arc change on a ≥ 1 –2 week timescale for observations of a given pulsar at one frequency. Hence, contemporaneous

observations (separated by a few days) should be satisfactory in assessing the bandwidth of an arc.

The data we display in Figures 2–4 show that scintillation arcs are a broadband phenomenon. For PSR B1929+10 (Fig. 2), a sharp arc boundary is present from 430 to 1175 MHz, and a weak arc is visible at ~ 1400 MHz. PSR B1133+16 (Fig. 3) has a more complicated scintillation arc structure, displaying a range of power at 430 MHz, two nested arcs at intermediate frequencies (1175 and 1400 MHz), and a faint trace of the inner arc at the highest frequency (2250 MHz). This pulsar has shown a wide variety of arc structure over the last 2 decades (S03). At some epochs only one arc is visible; at others as many as four nested arcs are present. This pulsar also goes through epochs in which the arc pattern breaks up into a rich array of inverted subarcs and other complicated substructure. In 2002 June, the pattern of twin arcs shown here persisted for 2 weeks and was identifiable as such in all but the highest frequency observation, in which sensitivity (or spectral development of the outer arc relative to the inner one) caused only the inner arc to be visible. These multifrequency observations over a 5 day span are much more similar to each other than to either previous or subsequent epochs.

In Figure 4 we see both time and frequency development for the arc structure of PSR B0834+06. Note that the data in Figure 4a were obtained 1.4 yr earlier than all the other data, which were taken in 2002 June; the data in Figure 4d were observed 2 weeks after the other June data. The most noticeable feature of the 2002 June observations is the left-right asymmetry of the power distribution, with the left-hand side of the figure having considerably more power in all cases. Although the details of the distribution change with frequency, this asymmetry persists over more than a factor of 3 in frequency. We note that the 1400 MHz

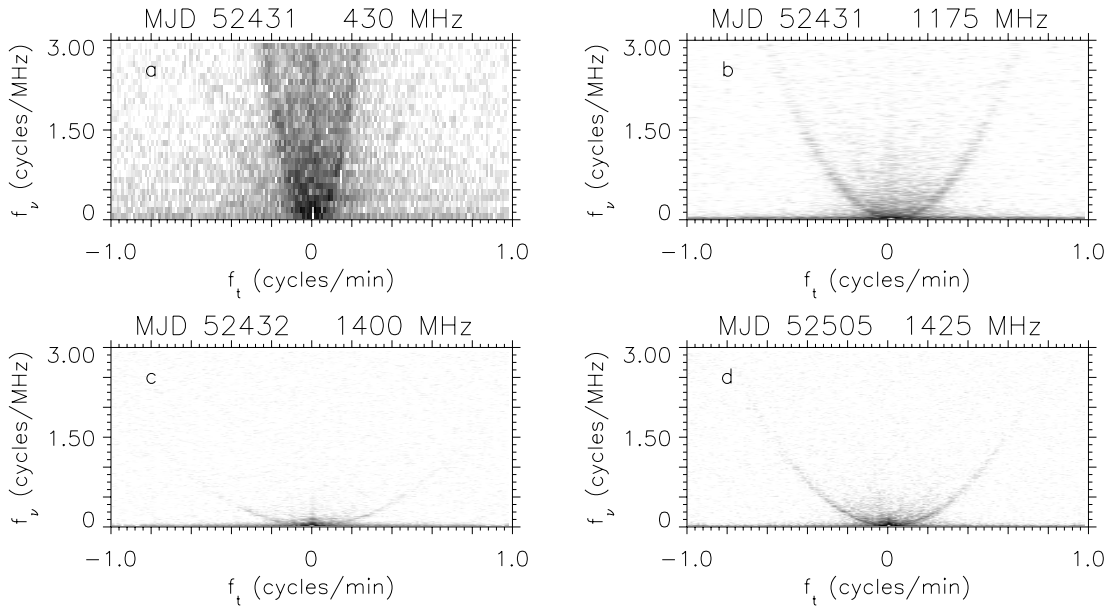


FIG. 2.—PSR B1929+10 secondary spectra at three frequencies. The secondary spectra are truncated to allow direct comparison of arc curvatures across the range of frequencies shown. The arc curvature decreases with increasing frequency. (a) A faint second arc is barely visible at 430 MHz, outside the main arc. The arc in (c) does not extend far from the origin, but it is sufficient to determine the curvature. Panel *d* shows an observation 3 months later to more clearly demonstrate the smaller curvature value at nearly the same frequency as in (c). The nonnegligible annual variation in $V_{\text{eff},\perp}$ for this pulsar requires a more detailed analysis, as discussed in the text.

observation (Fig. 4e) appears to be a contracted version (in both f_v and f_t) of the pattern at 1175 MHz (Fig. 4c), including a hint that the subarc at the upper left end of the power distribution (at $f_v \approx 1.5$ cycles MHz^{-1} in Fig. 4c, and $f_v \approx 0.7$ cycles MHz^{-1} in Fig. 4e) is present at both

⁷ The noise floors of the data in Figs. 4c and 4d are -54.2 dB and -53.4 dB, respectively, indicating that the larger extent of the arc features in Fig. 4d is not due to a significant difference in signal-to-noise ratio.

frequencies.⁷ The detailed tracing of subarc locations is beyond the scope of this paper and will be reported elsewhere. It is also worth noting that at 1175 MHz, the asymmetrical power distribution appears to expand outward in the secondary spectrum over the 14 day interval between the data in Figures 4c and 4d (note the difference in axis scales).

There is a systematic frequency development of the scintillation arcs that is visible in Figures 2–4. For arcs observed within a few days of each other, the 430 MHz observation

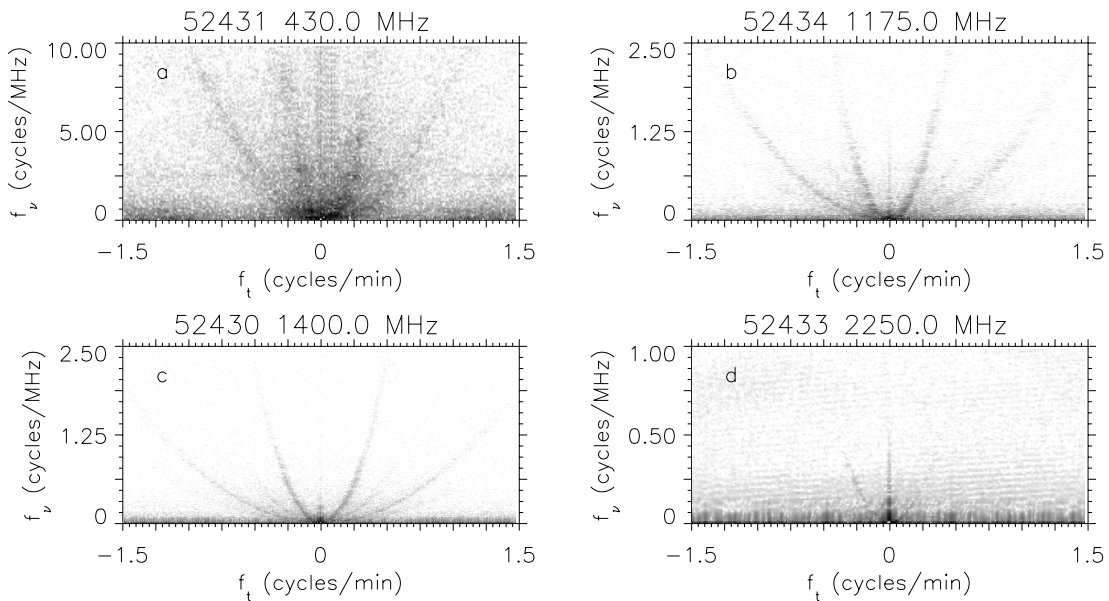


FIG. 3.—PSR B1133+16 secondary spectra at four frequencies. These four observations were taken in a 5 day span. As many as four arcs are visible for this pulsar; we determine the curvature separately for the two brightest arcs. Only the inner arc is visible at the highest frequency (2250 MHz). Note that the secondary spectra are truncated, and the scales are not the same for all observations. Each arc flattens out with increasing frequency.

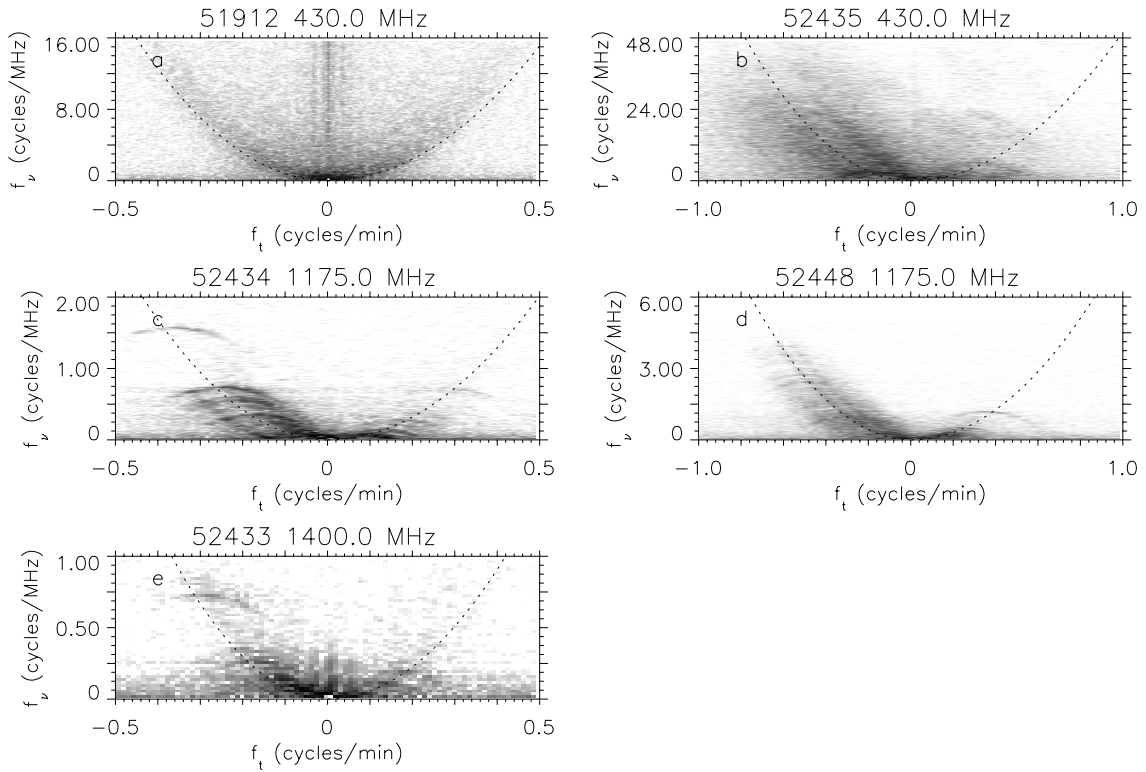


FIG. 4.—PSR B0834+06 secondary spectra at three frequencies. Panels *b*, *c*, and *e* are contemporaneous, whereas the data in (*a*) were obtained 1.4 yr earlier, and the data in (*d*) were observed 2 weeks later. The overplotted parabolas all have the same curvature, scaled to the appropriate frequency as $a \propto \nu^{-2}$. (The left and right sides are treated separately and have slightly different curvatures.) The inverted parabolic subarcs in (*c*), (*d*), and (*e*) are seen often for this pulsar and for several others in our monitoring program (S03). Note that the axis scales are set to show most of the detail in each observation.

consistently shows thicker and more diffuse arc structure than at the higher frequencies. In addition to this general trend, a new feature becomes clearly visible at higher frequencies for PSR B0834+06: the inverted subarc features mentioned above. Observations over a wider sample of pulsars and frequencies (S03) show that subarcs are often more prominent at higher frequencies, and that in general the main arc structure is thicker and more diffuse at 430 MHz.

For all three of these pulsars, then, we see that the general features of the scintillation arcs are continuous across a broad frequency range. Furthermore, the epoch-to-epoch changes are often large and random in character, compared to the more systematic development over frequency.

4.2. Arc Curvature Scaling

We investigated the relationship between the arc curvature parameter and observing frequency. Previously, we had found (S03) that the arc curvature does not vary appreciably at a single frequency over days or weeks, so it is safe to compare the arc curvature in observations spaced within a week of each other; all of our data for PSR B1929+10 and PSR B1133+16 meet this criterion. For PSR B0834+06, we used data from 2001 January in addition to the data from 2002 June. Since the velocity of this pulsar is much greater than the velocity of the observer ($V_{p\perp} = 174 \text{ km s}^{-1}$; Lyne, Anderson, & Salter 1982), we expect that $V_{\text{eff},\perp}$ is dominated by $V_{p\perp}$, implying that the arc curvature should not change substantially over the course of the year because of velocity effects.

We determined a using two methods. For all observations in this paper, we overplotted parabolas on the secondary

spectra with different curvature parameters and determined the best fit to the data by eye. We made multiple measurements of each arc (typically three to five) and used 3 times the standard deviation of those measurements to characterize the uncertainty. For some observations, we located points along the outer boundary of the scintillation arc and fitted those points to an equation of the form $f_\nu = af_t^2$. The two methods yielded consistent results, although the uncertainty in the former method was generally smaller because it uses all points along the scintillation arc to fit the parabola, instead of limiting the fit to a subsample of points. The a determinations used in this paper all use the overplotting method. We determined the arc curvature for negative and positive values of f_t separately and designate these as a_- and a_+ in Table 1, where we have also included the uncertainty in their determination.

Figure 2 shows secondary spectra for PSR B1929+10 over the frequency range 430–1425 MHz. The arcs are particularly well defined for this pulsar at all frequencies; at 430 MHz, there is significant power within the arc, but the edge is still bright, while the power is predominantly concentrated along the arc at the higher frequencies. The flattening of the arc with increasing frequency is easy to see. Note that the transverse velocity of this pulsar is small enough ($V_{p\perp} = 84 \text{ km s}^{-1}$; Brisken et al. 2002) that the orbital speed of the Earth is not negligible in comparison, implying that the curvature of the arc for this pulsar should change noticeably over the course of the year. Data showing this annual variation will be presented elsewhere; for this paper we use observations that were taken within a 3 day time span (Figs. 2*a*–2*c*), so $V_{p\perp}$ does not change substantially.

TABLE 1
ARC CURVATURE MEASUREMENTS

PSR	ν (MHz)	MJD	a_- (minutes ² MHz ⁻¹)	Error	a_+ (minutes ² MHz ⁻¹)	Error
B0834+06.....	430	51,912	71	7	64	6
B0834+06.....	1175	52,434	10.9	1.2	6.9	0.9
B0834+06.....	1175	52,448	9.3	0.8	8.8	1.0
B0834+06.....	1400	52,433	8.6	0.8	5.8	0.9
B1133+16 (outer).....	430	52,431	9.52	0.18	7.46	0.12
B1133+16.....	1175	52,434	1.18	0.06	1.06	0.03
B1133+16.....	1400	52,430	0.83	0.03	0.787	0.018
B1133+16 (inner).....	430	52,431	77	8	53	7
B1133+16.....	1175	52,434	11.0	0.6	9.7	0.4
B1133+16.....	1400	52,430	8.1	0.2	7.59	0.15
B1133+16.....	2250	52,433	3.3	0.4	3.0	0.4
B1929+10.....	430	52,431	47	4	47	2
B1929+10.....	1175	52,433	7.0	0.4	5.67	0.06
B1929+10.....	1400	52,432	4.6	0.4	4.6	0.2

NOTE.—For the pulsar PSR B1133+16, “outer” and “inner” refer to data for two distinct arcs.

Figure 3 shows secondary spectra for PSR B1133+16. As many as four arcs are visible for this pulsar, although we concentrate on the two brightest arcs (which we call the inner and outer arc in this study). Because of the sharper delineation of arcs at higher frequencies, the separate arcs are more obvious at 1175 and 1400 MHz. Only one arc is visible at 2250 MHz; its curvature is consistent with the curvature of the inner arc at lower frequencies, so we assume that only the inner arc is visible.

Secondary spectra of PSR B0834+06 are shown in Figure 4. We have observations of this pulsar, ranging from 430 to 1400 MHz, from the 2002 June observing run. However, the arc is too broad at 430 MHz in 2002 June (Fig. 4*b*) to accurately determine the curvature parameter. Because the power distribution of this pulsar was much less diffuse 1.4 yr earlier in 2001 January (Fig. 4*a*), we use that data to determine the curvature at 430 MHz. The overplotted parabolas in each 430 MHz observation have the same curvature, showing that the data are consistent with a being the same at both epochs despite the substantial thickening of the arc itself.

We determined a for each observation shown in Figures 2–4. The results for each pulsar are plotted as a function of frequency in Figure 5. Equation (8) predicts that $a \propto \nu^{-2}$. Figure 5, in which a single-parameter best-fit line of the predicted slope is drawn, shows that all of our observations are consistent with that prediction. Two-parameter fits of $\log a$ as a function of $\log \nu$ are shown in Table 2. Again, all the data are consistent with a slope of -2 , implying that a behaves as predicted by our model.

TABLE 2
 a vs. ν FITS

PSR	m	Error	b	Error
B1929+10.....	-2.08	0.10	7.1	0.3
B1133+16 (outer).....	-1.97	0.08	6.1	0.2
B1133+16 (inner).....	-1.77	0.09	6.5	0.3
B0834+06.....	-1.96	0.13	7.0	0.4

NOTES.—Bivariate linear fits to an equation of the form $\log_{10} a = m \log_{10} \nu + b$. The expected slope is $m = -2$.

5. DISCUSSION

As in other areas of astronomy, multifrequency observations are of great use in interpreting observations and maximizing the information obtained. We have shown that scintillation arcs are present contemporaneously at frequencies from 430 MHz to at least 1400 MHz, and in one case to 2200 MHz. This is important additional information to the understanding of the cause of scintillation arcs. With scattering-angle scaling as $\theta_{\text{scatt}} \propto \lambda^{2.2}$ for a Kolmogorov medium (Cordes, Pidwerbetsky, & Lovelace 1986), the 5:1 frequency range explored by these observations corresponds to more than a 30:1 ratio of angles contributing to the scintillation arcs at the highest and lowest frequencies. Several features, such as the left-right power asymmetry in PSR B0834+06 in Figure 4, are present over a large frequency range. This implies that the image features giving rise to the arcs must be similar over a wide range of angular scales. In turn, this points to coherent structures in the ISM that must be many times the size of the scattering disk (at the lowest frequency), since the scattering disk is conventionally related to the core of the image, whereas features in the wings of the scintillation arcs arise from scattered rays much farther out in the image. Preliminary analysis indicates that image anisotropy may be important to producing substructure in scintillation arcs (R03; M. Walker 2003, private communication); this, in turn, could be caused by anisotropic turbulence in the ISM due to a magnetic field (Higdon 1984; Higdon 1986; Goldreich & Sridhar 1995).

Our model for arc production is based on interstellar scattering dominated by one or several thin screens, leading to an image geometry with a bright central core surrounded by a weaker, extended halo. This model predicts that the arc curvature $a \propto \lambda^2$, which is confirmed by these observations. Note that the λ^2 scaling of arc curvature in equation (8) does not depend on the wavelength dependence of the scattering angle. Instead, it is due to the explicit λ^{-1} scaling in equation (1), which, once equation (1) is squared, gives rise to the λ^2 scaling in equation (8). The scattering angles present in equations (1) and (2) cancel each other out on the arc boundary, regardless of their scaling with wavelength.

Secondary spectra provide a powerful tool for probing the ISM along the line of sight to a pulsar. The presence of

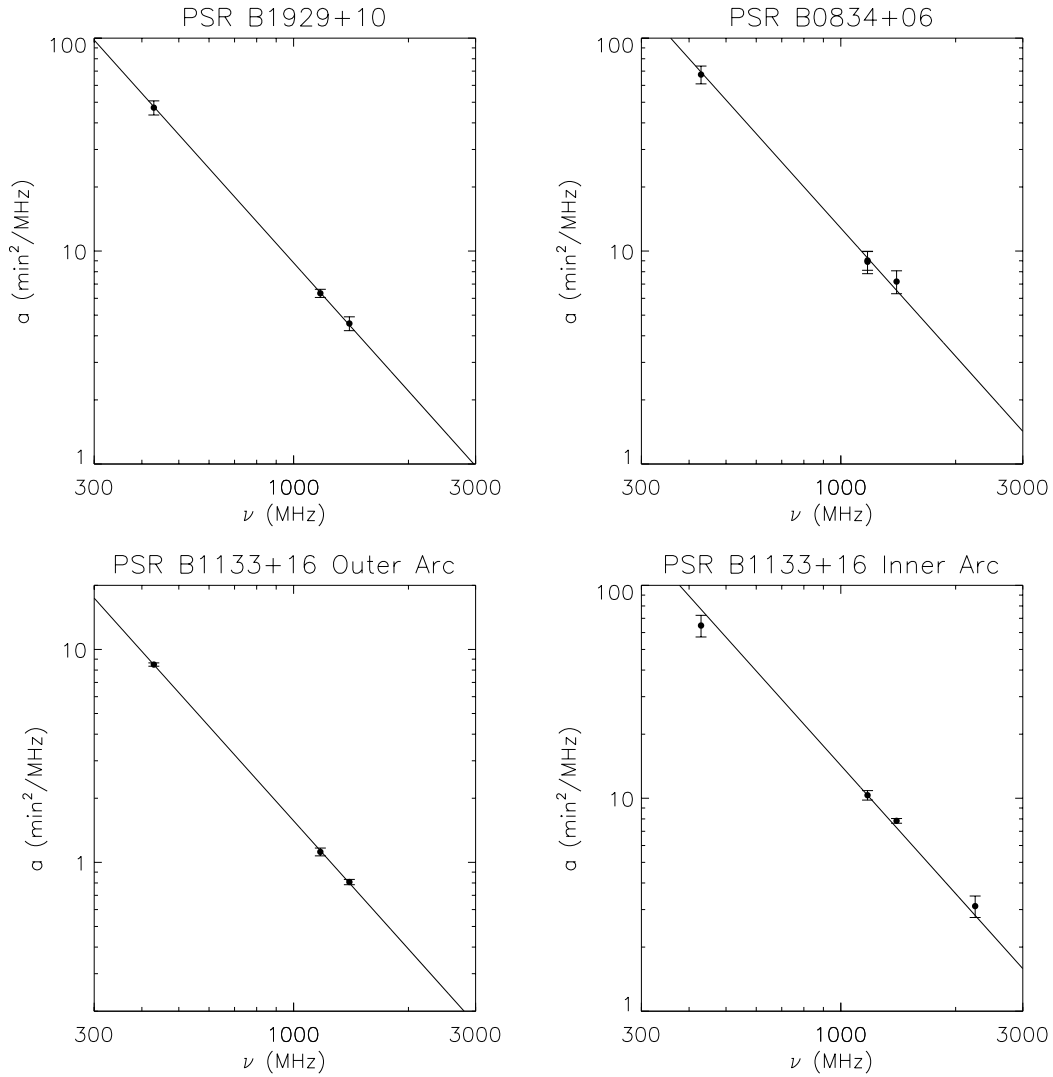


FIG. 5.—Curvature parameter values for PSR B1929+10, PSR B0834+06, and two arcs of PSR B1133+16, plotted as a function of observing frequency on a log-log plot. The unweighted mean of a_- and a_+ for each observation is shown. A line of the expected logarithmic slope (-2) is also shown for each plot; it represents a one-parameter (intercept) least-squares fit to the data. Two-parameter least-squares fits to the data are shown in Table 2; all are consistent with a logarithmic slope of -2 .

parabolic arcs requires that the scattering occur predominantly in one or several thin screens. In equation (8), a depends on the observing frequency, the pulsar distance and proper motion velocity, and the placement of the thin screen. Therefore, arc curvature can be used to determine the screen placement at any observing frequency, and we can combine observations at different frequencies to improve our determination of screen placement, as well as to explore substructure and asymmetry in the arcs.

The resolving power of scintillation analysis is impressive, as has been recognized for some time (e.g., Cordes & Wolszczan 1986). Scintillation arcs often possess a variety of substructure over a wide range of angular scales in high-sensitivity observations and hence provide new opportunities for analysis. We pursue this work in detail elsewhere, but an example here will be useful. Detailed substructure is seen in the secondary spectra of PSR B0834+06 in Figure 4. We can relate $\theta_{2x} - \theta_{1x}$ to values of f_i through equation (1) and known pulsar parameters. Using values of $V_{p\perp} = 174 \text{ km s}^{-1}$ (Brisken et al. 2002) and $\sigma = D_s/D = 0.33$ (S01), a

value of, e.g., $f_i = 1.0 \text{ cycles minute}^{-1}$ corresponds to $\theta_{2x} - \theta_{1x} = 6.8 \text{ mas}$ at 430 MHz, 2.5 mas at 1175 MHz, and 2.1 mas at 1400 MHz. At the inferred distance of the screen from the Earth of $D(1 - \sigma) = 0.55 \text{ kpc}$, this corresponds to physical scales at the screen of 3.7, 1.4, and 1.1 AU, respectively. These are the largest coherent structures that could give rise to the observed features in the secondary spectrum. If the features are due to diffractive effects, the relevant scale is much smaller: $s \sim \lambda/\theta \sim 2 \times 10^7 \text{ m}$.

Additional features in the secondary spectrum provide further information about the scattering screen and the structure of the ISM on $\sim 1 \text{ AU}$ size scales. Multiple arcs, such as those of PSR B1133+16, indicate the presence of multiple thin screens (for which the screen placement can be determined individually). The breadth of the arc may provide information about the longitudinal extent of the scattering screen. More features and their implications for the ISM are discussed in S03 and R03.

Analysis of scintillation arcs has the potential to probe the ionized ISM over a wider simultaneous range of spatial

scales than is possible with many other techniques. Since scintillation arcs often possess rich substructure that is time variable, they provide a continuing probe of the medium. The power distribution in the secondary spectrum shows details about the core of the image, as well as features that are, in some cases, separated from the core by more than 20 times its diameter. In addition, the study of substructure over a practical frequency range of ~ 5 yields another factor of 30 or so in the range of scales being probed. Further understanding of the relation between features in the secondary spectrum and their time and frequency development will lead to a powerful single-dish probe of AU-scale features in the interstellar medium.

We thank the National Science Foundation for support of this research through grant AST 00-98561. We also thank Oberlin College students W. B. Everett, N. R. Hinkel, D. F. Reeves, and J. T. Solomon for assistance in the preparation of this paper. M. A. McLaughlin and D. R. Lorimer shared data analysis software with us. D. R. S. and D. E. B. acknowledge hospitality and support from the Australia Telescope National Facility during part of this work. We thank our colleagues W. A. Coles, J. M. Cordes, S. Johnston, D. B. Melrose, B. J. Rickett, and M. A. Walker for stimulating discussions about scintillation arcs. We thank an anonymous referee for numerous helpful comments that improved this paper.

REFERENCES

- Armstrong, J. W., Rickett, B. J., & Spangler, S. R. 1995, *ApJ*, 443, 209
 Brisken, W. F., Benson, J. M., Goss, W. M., & Thorsett, S. E. 2002, *ApJ*, 571, 906
 Cordes, J. M., Pidwerbetsky, A., & Lovelace, R. V. E. 1986, *ApJ*, 310, 737
 Cordes, J. M., & Rickett, B. J. 1998, *ApJ*, 507, 846
 Cordes, J. M., & Wolszczan, A. 1986, *ApJ*, 307, L27
 Goldreich, P., & Sridhar, S. 1995, *ApJ*, 438, 763
 Hewish, A., Wolszczan, A., & Graham, D. A. 1985, *MNRAS*, 213, 167
 Higdon, J. C. 1984, *ApJ*, 285, 109
 ———. 1986, *ApJ*, 309, 342
 Lyne, A. G., Anderson, B., & Salter, M. J. 1982, *MNRAS*, 201, 503
 Norman, C. A., & Ferrara, A. 1996, *ApJ*, 467, 280
 Rickett, B. J. 1990, *ARA&A*, 28, 561
 Rickett, B. J., Lyne, A. G., & Gupta, Y. 1997, *MNRAS*, 287, 739
 Scheuer, P. A. G. 1968, *Nature*, 218, 920
 Stinebring, D. R., McLaughlin, M. A., Becker, K. M., Espinoza Goodman, J. E., Kramer, M. A., Sheckard, J. L., & Smith, C. T. 2001, *ApJ*, 549, L97 (S01)
 Taylor, J. H., & Weisberg, J. M. 1989, *ApJ*, 345, 434